

Crystal Composition and Afterglow in Mixed Silicates: The Role of Melting Temperature

O. Sidletskiy,¹ A. Vedda,^{2,*} M. Fasoli,² S. Neicheva,¹ and A. Gektin¹

¹*Institute for Scintillation Materials NASU, 60 Lenin Avenue, 61001 Kharkiv, Ukraine*

²*Department of Materials Science, University of Milano-Bicocca, Via Cozzi 55, 20125 Milano, Italy*
(Received 5 February 2015; revised manuscript received 20 May 2015; published 18 August 2015)

Modern applications of scintillator materials demand cutting-edge performances and require often a response speed in the nanosecond time scale. Slow light emission causing an “afterglow” is, therefore, of considerable concern in the development of fast scintillators. The mechanism of afterglow emission in mixed Ce-doped oxyorthosilicate scintillators is investigated by means of time-resolved scintillation, thermally stimulated luminescence (TSL), and radio-luminescence measurements. Various Ce-doped $\text{Lu}_{2x}\text{Gd}_{2-2x}\text{SiO}_5$ oxyorthosilicate crystals (with x ranging from 0 to 1) and $\text{Lu}_{1.8}\text{Y}_{0.2}\text{SiO}_5$ grown by the Czochralski technique are considered. The detailed TSL analysis reveals that thermally assisted tunneling recombination of electrons trapped by oxygen vacancies with holes trapped by Ce luminescence centers occurs for all compositions. The reduction of the afterglow intensity by adding gadolinium or yttrium into the host is accompanied by a lowering of the traps concentration, as deduced by the TSL intensity. Such lowering of the oxygen vacancy concentrations is found to be correlated with the decrease of the melting temperature induced by gadolinium or yttrium content increase, which governs the oxygen vapor pressure. The occurrence of a similar mechanism also in other scintillators and its influence on carrier trapping is discussed.

DOI: 10.1103/PhysRevApplied.4.024009

I. INTRODUCTION

Ce-doped oxyorthosilicate single crystals like Lu_2SiO_5 (LSO), $\text{Lu}_{2x}\text{Y}_{2-2x}\text{SiO}_5$ (LYSO), Gd_2SiO_5 (GSO), and $\text{Gd}_2\text{Y}_{2-2x}\text{SiO}_5$ (GYSO) are materials of choice as scintillators in several applications like, for example, medical imaging [1], high-energy physics [2], and well logging [3]. Most of these applications require scintillators with a fast response in the nanosecond time scale and afterglow-free signals. Such strict requirements motivate material engineering studies aimed at finding the most suitable crystal compositions and doping conditions to obtain fast and efficient crystals [4].

The high light output and fast luminescence decay of Ce-doped oxyorthosilicates are related to a low concentration of lattice defects acting as *shallow* traps. This trap feature is at variance with other complex Ce-doped oxides, like aluminum garnets and perovskites, in which such traps delay the radiative recombination at Ce^{3+} emission centers and are responsible for slow scintillation decay components and low light yield [5,6]. Despite the negligible presence of slow scintillation tails in oxyorthosilicates, their practical utilization was prevented until now in fields where the signal-to-noise ratio of the scintillation response is crucial, like, for example, in most imaging applications. This complication is due to their intense afterglow, i.e., a luminescence signal extending over the millisecond time

scale and whose magnitude is up to several percent of the initial scintillation amplitude [7]. Such afterglow is linked to electron trapping by *deep* traps related to oxygen vacancies [8]. These traps are evidenced by intense thermally stimulated luminescence (TSL) peaks detected above room temperature (RT). In LSO and $\text{LYSO}:\text{Ce}$, their thermal depth calculated on the basis of TSL data is about 1 eV [9].

Indeed, the key role of oxygen vacancies as deep traps capturing electrons during irradiation was put in evidence by recent studies dealing with silicates as well as other materials pertaining to the broad class of oxide scintillators [8–11]. “Defect management” by materials scientists consists of understanding the role of defects in the optical properties and reducing their concentration by suitable crystal growth strategies. Research efforts along this line can, indeed, allow us to obtain materials with improved scintillation decay parameters. In the case of $\text{LYSO}:\text{Ce}$, codoping with divalent cations was found to reduce defects and improve the scintillation time response [12]. In parallel, crystals with mixed cation compositions were found to display very interesting properties. In a previous investigation, it was shown that $\text{Lu}_{2x}\text{Gd}_{2-2x}\text{SiO}_5$ (LGSO) crystals display a progressively lower afterglow signal by increasing the Gd content [4]. With regard to the physical mechanism underlying such behavior, the analysis of the existing data allows us *a priori* to select two main hypotheses. The much weaker afterglow in Gd-rich crystals could be due to either (i) the presence of a lower concentration of oxygen vacancies with respect to $\text{LSO}:\text{Ce}$ or (ii) the occurrence of different spatial distributions between

*Corresponding author.
anna.vedda@unimib.it

traps and luminescent activators leading to different radiative recombination probabilities in a tunneling recombination process, as observed for LSO [9].

In the present investigation, the mechanism of afterglow suppression in Gd-rich oxyorthosilicates is unveiled by an experimental approach involving the analysis of both TSL and afterglow measurements performed on a broad ensemble of LGSO crystals characterized by different Lu/Gd ratios, as well as on GSO:Ce, LSO:Ce, and LYSO:Ce. In parallel, the relative change of oxygen vacancy concentrations in the crystals is evaluated by taking into account the dependence of the oxygen vapor pressure in the growth atmosphere upon the melting temperature for all the considered compositions.

Finally, aiming to discuss the impact of melt evaporation and defect formation on scintillation properties, a general discussion is proposed considering the available data on light yield and melting temperature for scintillator compounds of different chemical nature.

II. EXPERIMENTAL CONDITIONS

A. Single-crystal growth

The LGSO:Ce single crystals are grown by the Czochralski technique using an Ir crucible under similar conditions and from the same batch of raw materials with 99.99% purity. For orthosilicates, the oxygen content in the growth atmosphere must be kept below 1–2 vol % because of Ir crucible oxidation. Other crucible materials are not appropriate because of a relatively low melting temperature (Pt) or the occurrence of chemical reactions with SiO₂ melt (W, Mo). Thus, in this case, an Ar + 0.3% O₂ growth atmosphere is chosen. LGSO samples with different stoichiometry ($x = 1, 0.75, 0.6, 0.55, 0.50, 0.4, 0.35, 0.20, 0.15, 0.1, 0.05,$ and 0) are considered. In the text, samples are denoted as LSO, LGSO75, etc. Moreover, LYSO crystal is grown under similar conditions.

Concerning the possible different concentrations of oxygen vacancies, it has to be noted that the overall quantity of such defects can be influenced by the melting temperature of a given composition. Melt evaporation is determined by the vapor pressure of the components above the melt, which, in turn, depends on the temperature. For mixed oxyorthosilicates, the differences in melting temperatures are relevant, since they range from 2050 K in Lu_{0.34}Gd_{1.66}SiO₅ up to 2320 K in LSO [13]. Strong oxygen deficiency in this type of crystal is suggested by the data on postgrowth thermal treatments of LSO:Ce, LYSO:Ce, YSO:Ce [14], and LGSO:Ce [15]. Light output in LSO:Ce, YSO:Ce, and LYSO:Ce is increased after annealing in air [14]. On the other hand, annealing treatments did not change significantly the functional properties of LGSO:Ce [15].

B. Evaluation of crystal composition

True Lu and Gd concentrations in mixed LGSO:Ce crystals are determined by the analytical lines of

Lu (2615 Å) and Gd (3350 Å) using a TRACE SCAN Advantage atomic emission spectrometer with inductively coupled plasma (ICP AES) by Thermo Jarrell Ash (USA) using the external standard method. The lattice parameters of LGSO samples are obtained by using a single-crystal diffractometer “Xcalibur 3” by Oxford Diffraction (Mo K α radiation, $\lambda = 0.71073$ Å) equipped with a graphite monochromator, a sapphire-3 CCD detector, ω/θ scanning in the range $2\theta \leq 90^\circ$, and accounting for absorption by equivalent reflections. Structure calculations are carried out using a SHELX-97 and WinGX software. Elementary cell parameters are refined by the Rietveld method from diffractograms obtained on powders of the same crystalline samples using a Siemens D500 powder diffractometer.

Cerium concentrations are determined by the atomic emission spectrographic method based on evaporation of the substance in an ac arc discharge and registration of the emitted radiation by a DFS-1 spectrograph. The Ce concentration in LGSO:Ce and GSO:Ce samples is 0.37 ± 0.08 at. %. The Ce concentrations in LSO:Ce and LYSO:Ce are 0.2 and 0.1 at. %, respectively.

C. Estimation of defect concentrations

The relative change of the oxygen-vacancy concentration in the crystals can be estimated using the simple relation between the oxygen partial pressure (P) and absolute temperature (T) derived from the Clausius-Clapeyron relation (Antoine’s equation) [16]:

$$\log_{10}P = A - [B/(T + C)], \quad (1)$$

where A, B, C are constants (the values for each material are presented, for example, in Ref. [17]).

The melting temperatures for all LGSO compositions are taken from Ref. [13], while the LYSO melting temperature is reported in Ref. [18]. Because of the previously suggested correspondence between traps and oxygen vacancies, the relative changes of TSL or afterglow intensities can correspond to the changes of the oxygen vapor pressure above the melt. Since the vapor pressures in lanthanide oxides are 2–3 orders of magnitude lower compared to SiO₂ [17], the evaporation of Lu₂O₃, Gd₂O₃, and Ce₂O₃ can be neglected, and it can be assumed that oxygen deficiency in the melt is caused solely by the evaporation of SiO₂ or of its dissociation products. Therefore, the temperature dependence of oxygen vapor pressure in LGSO:Ce can be evaluated inserting the coefficients for $\log_{10}P_{O_2}$ into Eq. (1). These coefficients [Eq. (2)] are determined separately for Si and O₂ in Ref. [17] for the temperature range from 1996 °C to 3000 °C by fitting the mass spectrometry data of dissociation products during SiO₂ evaporation:

$$\log_{10}P_{O_2} = -26462/T + 7.84. \quad (2)$$

D. Afterglow, radio-luminescence, and TSL measurements

TSL measurements after RT x-ray irradiation by a Machlett OEG 50 x-ray tube operated at 20 kV are performed from RT up to 400 °C with a linear heating rate of 1 °C/s using two different apparatuses. In the first one, the total emitted light is detected as a function of the temperature by photon counting using an EMI 9635 QB photomultiplier tube. The second apparatus is a specially designed high-sensitivity TSL setup [19] spectrometer measuring the TSL intensity as a function of both temperature and emission wavelength; the detector is a double-stage microchannel plate followed by a 512-diode array; the dispersive element is a 140-lines/mm holographic grating, the detection range being 200–800 nm. The spectral resolution is approximately 15 nm. TSL glow curves are corrected for the temperature dependence of the $5d_1-4f$ radiative transition of Ce^{3+} monitored by radio-luminescence (RL) measurements under x-ray irradiation ($V = 40$ kV, $I_a = 25$ mA, Cu anode).

Afterglow measurements after a specified delay time are carried out using a special setup with a pulsed x-ray emitter of RAPAN-200 type ($U = 130-140$ kV, $I_a = 3-4$ mA, W anode). A Hamamatsu S8594 photodiode, a current-to-voltage converter, a multiplexor and an analog-to-digital converter, a PC, a S1-102 oscilloscope, and a control block for the x-ray emitter are used for the tests. The electronic noise and natural isotopes background are subtracted. The temperature dependence of the RL signal integrated from 200 to 800 nm (containing the full Ce^{3+} $5d-4f$ emission spectral range) is measured under sample cooling from 150 to 425 K and irradiation by the same x-ray source; during the measurements, the temperature is recorded using a RP1-16A controller.

III. RESULTS

In Fig. 1 the afterglow measurements for “pure” (LSO and GSO) and mixed (LYSO and LGSO) oxyorthosilicates are shown. These data demonstrate a very clear signal reduction (more than 2 orders of magnitude) when moving from LSO to GSO.

The light detected after the x-ray excitation pulse is due to different contributions. In fact, besides the fast scintillation emission with a decay time in the order of tens of nanoseconds, the delayed recombination of carriers temporarily captured by shallow traps gives rise to slower decay components, in the order of a few milliseconds.

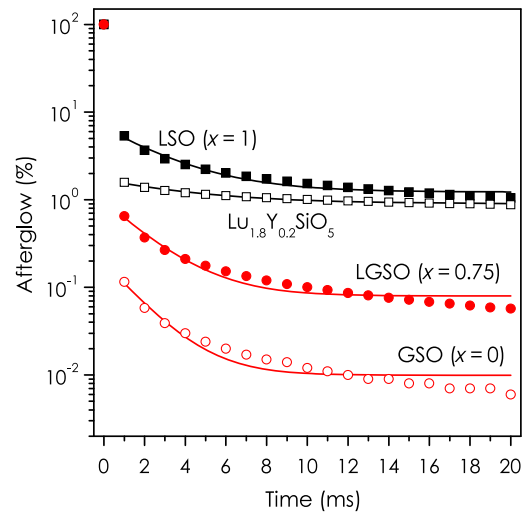


FIG. 1 Afterglow intensity in the millisecond time range (symbols) and exponential fits (curves) for some Ce-doped crystals under study.

This phenomenon is what can be properly called “afterglow.” Moreover, a constant background signal with a sample-dependent intensity is also detected. Such background is due to both electronic circuit noise and to ^{176}Lu isotope radioactivity. In order to isolate the afterglow, we must exclude both the contribution from the fast scintillation light and the background noise. For this reason, the afterglow experimental dependencies were fit from 1 to 20-ms, excluding the first millisecond, with the exponential decay equation $y = A \exp(-t/\tau) + y_0$. Then the equations $y = A \exp(-t/\tau)$ are integrated from 0 to 10^5 -ms (see Fig. 8) to exclude the contribution from the constant background which is accounted for by the y_0 parameter. The parameters obtained from the fit are presented in Table I.

The afterglow phenomenon is further investigated by means of wavelength-resolved TSL measurements. The TSL measurement obtained for LGSO:Ce with 50 at. % Lu (Fig. 2) shows that the emission is clearly dominated by the $5d_1-4f$ transition of Ce^{3+} . No traces of Gd^{3+} emission around 315 nm or of other bands are revealed.

The TSL glow curves above RT of LGSO samples are shown in logarithmic scale in Fig. 3. In this case, the TSL intensity is measured by photon counting using an EMI 9635 QB photomultiplier. Glow peaks at approximately 80 °C, 130 °C, 180 °C, and 240 °C are observed. These peaks, previously attributed to thermally assisted tunneling

TABLE I. Fit parameters of the afterglow curves.

x in $Lu_{2x}Gd_{2-2x}SiO_5$	1	0.75	0.6	0.55	0.4	0.35	0.2	0.15	0.1	0.05	0	LYSO
y_0	1.22	0.08	0.02	0.027	0.040	0.022	0.015	0.02	0.031	0.02	0.01	0.89
A	5.46	0.88	0.45	0.39	0.58	0.36	0.19	0.69	0.47	0.3	0.18	0.79
τ (ms)	2.89	2.06	1.72	1.86	1.88	1.79	1.97	1.46	1.84	1.88	1.70	4.64

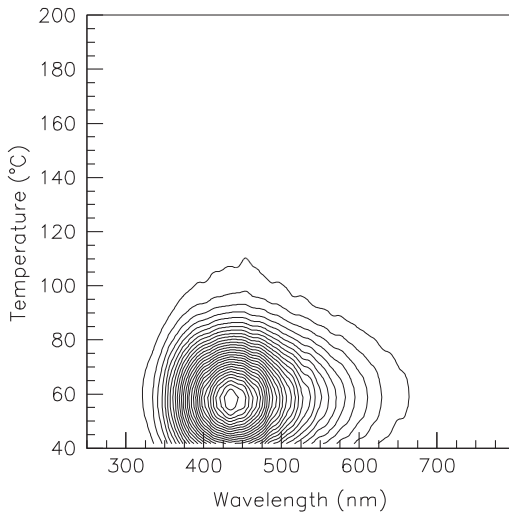


FIG. 2 Contour plot of a wavelength-resolved TSL measurement performed on the LGSO50 sample after RT x-ray irradiation. The TSL intensity is reported in linear scale. For this reason, only the main signal below 120°C is evident.

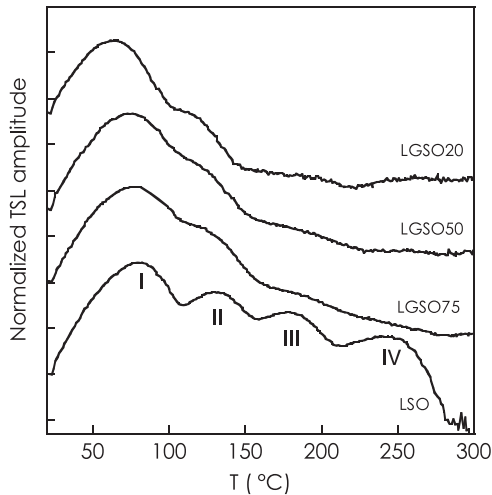


FIG. 3 TSL glow curves in logarithmic scale of all samples following x-ray irradiation at RT normalized to their maximum values. The curves are shifted on the ordinate scale for better clarity.

from oxygen vacancies to Ce centers [9], are detected for all Lu concentrations, although they become progressively less defined as the Gd concentration increases. However, the peak at 300°C due to electron detrapping via the conduction band and detected in LYSO:Ce [9] is not observed in any of the samples.

The effect of the Lu and Gd content on the trap concentrations is investigated in different samples by comparing the glow curves obtained with the same irradiation dose (0.02 Gy). The TSL intensity depends on the trap concentrations (being the concentration of recombination centers approximately the same for all of the samples) and the efficiency of the Ce³⁺ luminescent center, which

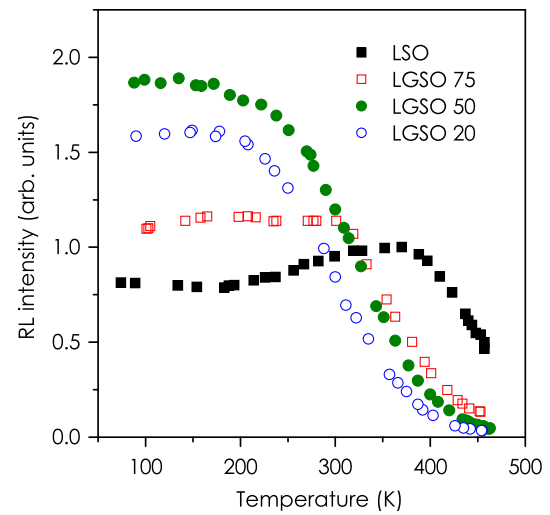


FIG. 4 Temperature dependence of RL intensity for all samples studied by TSL.

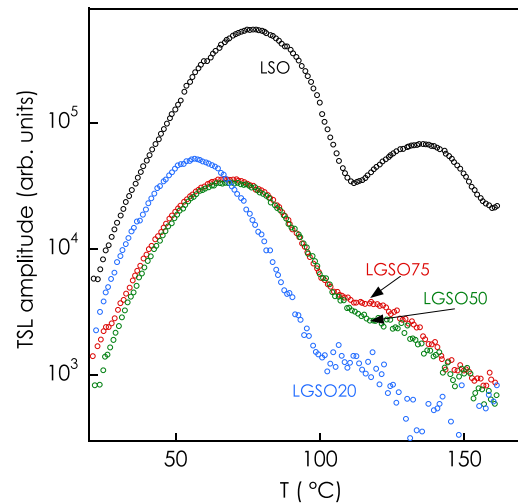


FIG. 5 TSL glow curves of all samples corrected for the RL temperature dependence.

is evaluated by RL measurements versus temperature (Fig. 4).

Therefore, each glow curve is corrected by dividing it by the corresponding RL efficiency versus temperature. Since the RL temperature dependence can be obtained only up to 180°C, the correction can be performed only for the first two principal TSL peaks at 80°C and 130°C. The corrected glow curves are presented in Fig. 5.

The glow curves in LGSO:Ce are weaker by over 1 order of magnitude with respect to LSO. A strong reduction of TSL is observed already after the introduction of 25% of Gd, while the TSL intensity keeps almost constant with further Gd addition. Therefore, the TSL intensity seems to be correlated with the one of afterglow.

IV. DISCUSSION

In accordance with previous investigations, the presence of the strong afterglow in orthosilicates relates to a high concentration of oxygen vacancies acting as deep electron traps [8,9]. In conditions of oxygen deficiency in the melt, the formation of oxygen vacancies should be energetically more favorable at oxygen sites which do not belong to SiO_4 tetrahedra [9]. There are 20% non-silicon-bound oxygen atoms in the monoclinic $C2/c$ structure of LSO, LYSO, and $\text{Lu}_{2-x}\text{Gd}_x\text{SiO}_5$ ($x < 1.6$) [20]. The bonds of these oxygens with Gd and Lu in LGSO are weak because their length is above 2.6 Å versus 1.6 Å for Si–O. A remarkable feature is that while a very intense afterglow is observed in LSO:Ce [8], the afterglow is very weak in GSO:Ce and GYSO:Ce [21] possessing a different type of monoclinic structure ($P2_1/c$) though with the same fraction of non-silicon-bound oxygen atoms [20] and with similar distances between the lanthanide and its oxygen environment.

Other than the presence of a lower concentration of oxygen vacancies in GSO with respect to LSO and LYSO, as mentioned above, the occurrence of a different spatial distribution between traps and luminescent activators can be taken into account to justify a lower afterglow intensity. In the following, we analyze TSL data in order to discuss such a possibility. Indeed, thermally assisted tunneling of electrons between traps and activators is found to occur in the TSL recombination of Ce-doped LSO and LYSO [9], similar to Lu–Y perovskites [10]. This mechanism is strongly distance dependent and occurs efficiently for trap-center distances up to a few angstroms. The introduction of a larger ion like Ce^{3+} into the LSO (LYSO) lattice could lead to its spatial correlation with oxygen vacancies. In fact, the probability of defect formation is higher near Ce^{3+} ions, since it induces slight lattice distortions, thereby promoting the thermally assisted tunneling recombination and afterglow. Both the afterglow suppression and the improvement of light yield achieved by isovalent doping with Gd^{3+} in LGSO:Ce mixed crystals [4] can be ascribed to a similar cause. Large quantities of Gd or similarly larger trivalent cations can efficiently attract those defects (oxygen vacancies) usually found spatially correlated with cerium. Therefore, even though the defect concentration is not reduced, most of them can be located near Gd^{3+} whose concentration is approximately 2 orders of magnitude larger than that of Ce^{3+} . As a result, electron traps might be located too far from Ce^{3+} for an efficient tunneling recombination to occur.

The trap parameters are evaluated by means of TSL analysis. In particular, the trap depths are estimated using the “initial rise” method after partial cleaning of the glow peaks, as described in Ref. [22]. In this case, the RL temperature dependence curve allows us to correct the initial portion of all of the glow peaks (in fact, the initial rise of even the highest temperature peak lies well below 180 °C). A similar value of 1.0 eV with an uncertainty

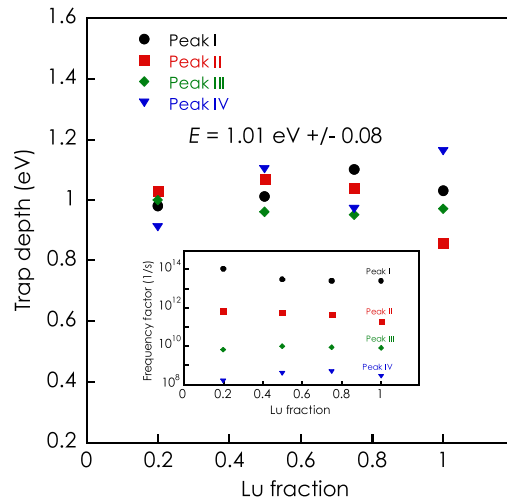


FIG. 6 Trap depths evaluated by the initial rise method for peaks I–IV on all samples. The inset reports the corresponding frequency factors of the traps. The standard deviation for the frequency factors is approximately 50%.

lower than 10% (Fig. 6) is obtained for all of the TSL peaks and all of the samples. The frequency factors s of the TSL peaks are then calculated from the formula

$$\frac{\beta E}{kT_m^2} = s \exp\left(\frac{-E}{kT_m}\right). \quad (3)$$

In a thermally assisted tunneling process, the frequency factor s can be expressed as [23]

$$s = x\nu_T \exp\left(\frac{\Delta S}{k}\right), \quad (4)$$

where x is the transmission coefficient of the barrier, ν_T is the thermal vibration frequency, and $\Delta S/k$ is an entropy factor. The transmission coefficient x takes the form [22]

$$x = \exp(-\varphi r), \quad (5)$$

where φ is a constant, and r is the trap-to-center distance.

Frequency factors are plotted as a function of oxygen-lanthanide (O–Ln) distances (r) in the LnO_7 polyhedron of the monoclinic $C2/c$ structure (Fig. 7).

The data display an exponential dependence upon the O–Ln distance. Therefore, the TSL measurements and their analysis show that the same thermally assisted tunneling recombination mechanism operates for all crystal compositions, indicating that a similar spatial correlation between traps and Ce centers occurs in all samples despite the presence of high concentrations of Gd ions in some of them.

Figure 8 reports the dependence of oxygen vapor pressure P from the melting temperature T_m based on

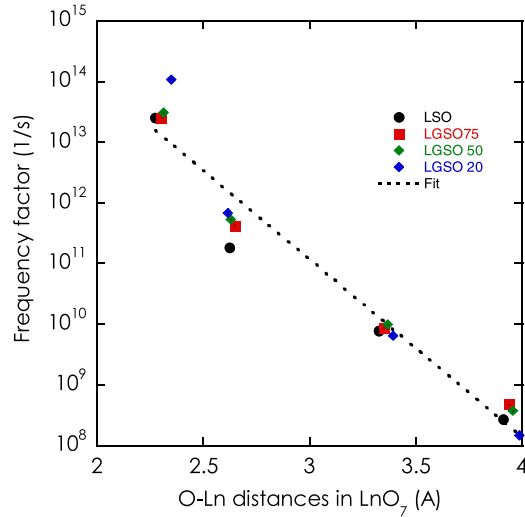


FIG. 7 Dependence of the frequency factors upon the first Ln-O distances in LGSO derived from XRD. The dotted line represents the fit of the data according to an exponential function (see text).

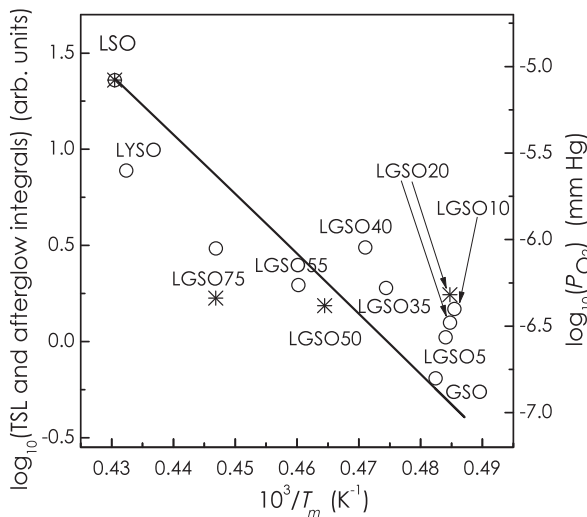


FIG. 8 Arrhenius plot of the integrals of TSL curves reported in Fig. 5 (asterisks, left scale), of the afterglow integrals from 0 to 10^5 -ms (hollow symbols, left scale), and of SiO_2 vapor pressure (continuous line, right scale) vs the reciprocal of melting temperature. Both TSL and afterglow integrals are affected by a standard deviation of approximately 20%.

Eq. (2) (see Sec. II C). In the graph, the integrals of the TSL curves shown in Fig. 5, as well as those of the afterglow curves, are also reported. Both these data appear to be qualitatively proportional to the oxygen vacancy concentrations in the crystals. A qualitative correspondence between P and experimental TSL and afterglow points is evidenced, indicating that melt evaporation significantly affects the trap concentration and afterglow in LGSO:Ce.

A perfect coincidence between the points and the analytical curve for LSO and GSO can be noted, while data points corresponding to the mixed crystals show a

higher spread. This spread can be attributed to another kind of mechanism, for example, the decrease of carrier thermalization length due to inhomogeneities and/or electron-phonon interaction in mixed crystals [24]. The trend is also somewhat different for crystals with monoclinic $C2/c$ and $P2_1/c$ (the points for GSO and for $x = 0.05-0.1$).

The analysis reveals that the decrease of both TSL intensity and afterglow is due to the lowering of oxygen vacancy concentration by increasing the Gd content in the lattice. The reduction of the number of oxygen vacancies is due to the drop of the melting temperature and subsequent decrease of the melt evaporation. At the same time, in analogy with previous results on LSO:Ce and LYSO:Ce, the presence of four glow peaks with the same trap depth detected in LGSO is interpreted as being due to the presence of a single-electron trap (oxygen vacancy) located at different distances with respect to Ce^{3+} recombination centers. The radiative recombination between electrons and holes occurs through a thermally stimulated tunneling mechanism. Therefore, the TSL results in conjunction with vapor pressure data rule out the hypothesis that afterglow differences can be due to variations of trap-center spatial distributions in Gd-rich samples.

Mixed cation composition as a strategy to improve the optical properties of scintillators was recently employed in the case of garnets. For $(\text{Lu})_3(\text{Ga}, \text{Al})_5\text{O}_{12}$ and $(\text{Lu}, \text{Gd})_3(\text{Ga}, \text{Al})_5\text{O}_{12}$, in a band-gap engineering approach, the introduction of Ga above 20 mol % is found to vary the position of trap levels with respect to the valence and conduction band, thus, reducing their influence on scintillation [25,26]. Additional codoping with divalent cations was also employed in order to tune the valence state of Ce and improve the scintillation performances [27,28].

Because of the adoption of a mixed Lu, Gd crystal composition, the performances of crystalline silicates are significantly improved, as is evidenced by the comparison of several practical scintillation parameters of $\text{Lu}_{0.6}\text{Gd}_{1.6}\text{SiO}_5:\text{Ce}$ taken as an example with those of other scintillators for x-ray CT reported in Table II. In particular, the afterglow (and, hence, the signal-to-noise ratio defined as its inverse) is very significantly improved in $\text{Lu}_{0.4}\text{Gd}_{1.6}\text{SiO}_5:\text{Ce}$ with respect to LYSO and LSO, without worsening the other parameters apart from some reduction of the density of the material. Moreover, from Table II, it appears that LGSO possesses the lowest afterglow level also in comparison to the other scintillator structures. This paves the way for the use of these crystals in applications in which the signal-to-noise ratio is a demanding parameter as in modern medical diagnostic techniques like computed tomography and positron emission tomography.

The correlation found here between the carrier trapping and melting temperatures raises the question of the occurrence of a similar mechanism also in other scintillation

TABLE II. Parameters of Ce-doped LGSO, LYSO, and LSO in comparison with the literature data on main scintillators in x-ray CT [29,30].

Scintillator	Density (g/cm ³)	Relative light output (%)	Emission maximum (nm)	Primary decay (μ s)	Afterglow (% at 3 ms)	Signal-to-noise ratio
CdWO ₄	7.9	100	530	2, 15	0.1	1000
CsI:Tl	4.51	330	550	1	>0.3	330
(Y, Gd) ₂ O ₃ :Eu	5.9	152	610	1000	5	20
Gd ₂ O ₂ S:Pr, Ce	7.34	180	520	2.4	0.1	1000
Gd ₂ O ₂ S:Tb(Ce)	7.34	180	550	600	0.7	140
Gd ₃ Ga ₅ O ₁₂ :Cr, Ce	7.09	138	730	150	0.1	1000
Lu_{0.4}Gd_{1.6}SiO₅:Ce	6.55	52	420	0.05	0.05	2000
LYSO:Ce	7.1	50	420	0.04	1.3	77
(reference)						
LSO:Ce (reference)	7.4	35	420	0.04	2.9	34

TABLE III. Melting temperatures and light yields of some scintillation crystals. L_{LT} and L_{HT} denote light yields of low-temperature and high-temperature compounds in the pair, respectively.

Compounds	YAlO ₃ :Ce	Y ₃ Al ₅ O ₁₂ :Ce	Y ₃ Al ₅ O ₁₂ :Pr	Y ₂ SiO ₅ :Ce	MgWO ₄
	LuAlO ₃ :Ce	Lu ₃ Al ₅ O ₁₂ :Ce	Lu ₃ Al ₅ O ₁₂ :Pr	Lu ₂ SiO ₅ :Ce	ZnWO ₄
<i>Melting temperatures (K)</i>	2143	2223	2223	2243	1493
	2203	2253	2253	2323	1631
L_{LT} - L_{HT} (photons/MeV)	18 000	16 700	16 000	27 500	5500
	11 400	12 500	17 000	20 500	8000
L_{LT}/L_{HT}	1.6	1.3	~1	1.4	0.7

Compounds	LaCl ₃ :Ce	BaBr ₂ :Eu	SrI ₂ :Eu	CsBa ₂ Br ₅ :Eu	Bi ₄ Si ₃ O ₁₂
	LaBr ₃ :Ce	BaI ₂ :Eu	BaI ₂ :Eu	CsBa ₂ I ₅ :Eu	Bi ₄ Ge ₃ O ₁₂
<i>Melting temperatures (K)</i>	1001	984	807	883	1303
	1121	1130	984	915	1323
L_{LT} - L_{HT} (photons/MeV)	50 000	58 000	1 12 000	1 02 000	2000
	75 000	40 000	58 000	92 000	8000
L_{LT}/L_{HT}	0.7	1.45	1.9	1.1	0.25

compounds. A concise answer to this question cannot be formulated because of the small quantity of available TSL and/or afterglow data measured under the same conditions and using samples obtained by a similar procedure. Keeping in mind that carrier trapping and afterglow intensity usually change reciprocally with respect to light yield, the comparison between light yields and melting temperatures can be used as an alternative. Such comparison is proposed in Table III where data related to several pairs of materials with the same chemical nature and crystalline structure but different melting temperatures are resumed. Here we did not include mixed crystals like LGSO:Ce where other scintillation mechanisms, for example, light-yield improvement due to limitation of carrier thermalization length by crystal inhomogeneities [24], may mask the discussed effect. The scintillation yields and melting points are taken from Ref. [30] and references therein, as well as from Refs. [4,18,24,31–34].

The majority of the Ce³⁺-, Pr³⁺-, or Eu²⁺- activated compounds show a light yield increase by 1.1–1.9 times

when the melting temperature is reduced, supporting the assumption that carrier-trap concentration decreases by the melting-temperature decrease. The only exception is the LaBr₃:Ce/LaCl₃:Ce pair, while in Lu₃Al₅O₁₂:Pr/Y₃Al₅O₁₂:Pr, the melting temperatures and light yields are similar. Interestingly, both pairs of scintillators with self-activated luminescence, ZnWO₄/MgWO₄ and Bi₄Ge₃O₁₂/Bi₄Si₃O₁₂, respectively, display an opposite trend. Since the host tungsten and bismuth oxyanions are the responsible centers for luminescence in these compounds, the luminescence centers concentration is 2–3 orders of magnitude larger compared to that of rare-earth-activated scintillators. For this reason, the carrier mean free path to the luminescence center should be smaller in self-activated compounds and, probably, in these cases the scintillation process is less sensitive to the presence of lattice defects.

We note that care must be taken in this comparison between light yields and melting temperatures since, indeed, other factors like the band-gap values, as well as

the positions of the energy levels of the activators and traps in the band gaps, can influence the light yields. Concerning band-gap values, we fail to find clear correlations between their variations and light yields in the same pairs of compounds [35–44]. Since the band-gap values reported in the literature are quite often contradictory, this correlation deserves further study.

V. CONCLUSIONS

Our investigation proves that modification of oxygen-vacancy concentration induced by Gd introduction causes afterglow suppression in mixed $\text{Lu}_{2x}\text{Gd}_{2-2x}\text{SiO}_5$ orthosilicate scintillators. A similar effect is found also for $\text{Lu}_{1.8}\text{Y}_{0.2}\text{SiO}_5:\text{Ce}$. Therefore, the introduction of Gd or Y cations allows us to decrease the oxygen vacancy concentration, i.e., decrease the carrier trap concentrations and reduce the storage of free carriers created during irradiation by ionizing beams. The effect is related to a reduction of melting temperature bringing a decrease of the melt evaporation.

The recent use of a mixed cation composition in garnet scintillators allows the tuning of the position of defect levels with respect to the valence and conduction bands and, hence, reduces their trapping effect. Interestingly, the case of silicates is an example in which the mixing of Lu and Gd cations is found to work in a different way, providing a reduction of the concentration of trap levels due to oxygen vacancies. Such a strategy can apply to all crystalline structures in which a significant lowering of the melting temperature occurs with respect to the simple one-cation composition. Because of this mechanism of defect reduction, mixed orthosilicate crystals acquire favorable properties for modern medical imaging applications.

Finally, from a broad comparison between light yield and melting temperature data of several crystals, it is evidenced that defect formation due to nonstoichiometric melt evaporation is an important factor affecting scintillation performance in rare-earth-activated scintillators. This finding should inspire further engineering approaches of novel scintillation compounds with high light yield and low trap concentration.

ACKNOWLEDGMENTS

The authors are grateful to Dr. K. Katrunov and Mr. Igor Zenya (ISMA NAS of Ukraine) for providing RL measurements and to Dr. V. Baumer (SSI “Institute for Single Crystals” NAS of Ukraine) for XRD data.

[1] C. L. Melcher, Scintillation crystals for PET, *J. Nucl. Med.* **41**, 1051 (2000).

[2] J. Chen, L. Zhang, and R.-Y. Zhu, Large size LYSO crystals for future high energy physics experiments, *IEEE Trans. Nucl. Sci.* **52**, 3133 (2005).

- [3] A. Nikitin and S. Bliven, Needs of well logging industry in new nuclear detectors, *IEEE Nucl. Sci. Symp. Conf. Rec.*, doi:10.1109/nssmic.2010.5873961 (2010).
- [4] O. Sidletskiy, A. Belsky, A. Gektin, S. Neicheva, D. Kurtsev, V. Kononets, D. Dujardin, K. Lebbou, O. Zelenskaya, V. Tarasov, K. Belikov, and B. Grinyov, Structure-property correlations in a Ce-doped $(\text{Lu}, \text{Gd})_2\text{SiO}_5:\text{Ce}$ scintillator, *Cryst. Growth Des.* **12**, 4411 (2012).
- [5] M. Nikl, A. Vedda, M. Fasoli, I. Fontana, V. V. Laguta, E. Mihokova, J. Pejchal, J. Rosa, and K. Nejezchleb, Shallow traps and radiative recombination processes in $\text{Lu}_3\text{Al}_5\text{O}_{12}:\text{Ce}$ single crystal scintillator, *Phys. Rev. B* **76**, 195121 (2007).
- [6] A. Vedda, M. Fasoli, M. Nikl, V. V. Laguta, E. Mihokova, J. Pejchal, A. Yoshikawa, and M. Zhuravleva, Trap-center recombination processes by rare earth activators in YAlO_3 single crystal host, *Phys. Rev. B* **80**, 045113 (2009).
- [7] R. Visser, C. L. Melcher, J. S. Schweitzer, H. Suzuki, and T. A. Tombrello, Photostimulated luminescence and thermoluminescence of LSO scintillators, *IEEE Trans. Nucl. Sci.* **41**, 689 (1994).
- [8] P. Dorenbos, C. W. W. van Eijk, A. J. J. Bos, and C. L. Melcher, Afterglow and thermoluminescence properties of Lu_2SiO_5 scintillation crystals, *J. Phys. Condens. Matter* **6**, 4167 (1994).
- [9] A. Vedda, M. Nikl, M. Fasoli, E. Mihokova, J. Pejchal, M. Dusek, G. Ren, C. R. Stanek, K. J. McClellan, and D. D. Byler, Thermally stimulated tunneling in rare-earth doped Lu-Y oxyorthosilicates, *Phys. Rev. B* **78**, 195123 (2008).
- [10] A. Vedda, M. Martini, F. Meinardi, J. Chval, M. Dusek, J. A. Mares, E. Mihokova, and M. Nikl, Tunneling process in thermally stimulated luminescence of mixed $\text{Lu}_x(\text{Y}^{3+})_{1-x}\text{AlO}_3:\text{Ce}$ crystals, *Phys. Rev. B* **61**, 0801 (2000).
- [11] V. V. Laguta, M. Martini, A. Vedda, E. Rosetta, M. Nikl, E. Mihokova, and Y. Usuki, Electron traps related to oxygen vacancies in PbWO_4 , *Phys. Rev. B* **67**, 205102 (2003).
- [12] S. Blahuta, A. Bessi re, B. Viana, P. Dorenbos, and V. Ouspenski, Evidence and consequences of Ce^{4+} in $\text{LYSO}:\text{Ce}$, Ca and $\text{LYSO}:\text{Ce}$, Mg single crystals for medical imaging applications, *IEEE Trans. Nucl. Sci.* **60**, 3134 (2013).
- [13] M. Glowacki, G. Dominiak-Dzik, W. Ryba-Romanowski, R. Lisiecki, A. Strzep, T. Runka, M. Drozdowski, V. Domukhovski, R. Diduszko, and M. Berkowski, Growth conditions, structure, Raman characterization and optical properties of Sm-doped $(\text{Lu}_x\text{Gd}_{1-x})_2\text{SiO}_5$ single crystals grown by the Czochralski method, *J. Solid State Chem.* **186**, 268 (2012).
- [14] B. Chai, Method of enhancing performance of cerium doped lutetium yttrium orthosilicate crystals and crystals produced thereby, U.S. Patent No. 7,166,845 B1 (Jan 23, 2007).
- [15] D. Kurtsev, O. Sidletskiy, S. Neicheva, V. Bondar, O. Zelenskaya, V. Tarasov, M. Biatov, and A. Gektin, LGSO:Ce scintillation crystal optimization by thermal treatment, *Mater. Res. Bull.* **52**, 25 (2014).
- [16] C. Antoine, Tensions des vapeurs; nouvelle relation entre les tensions et les temp ratures, *C.R. Hebd. Seances Acad. Sci.* **107**, 681 (1888).

- [17] I. S. Kulikov, Handbook, "Termodinamika Oksidov" (Thermodynamics of Oxides) (Izd. Metallurgiya, Moscow, 1986), p. 101.
- [18] <http://www.epic-crystal.com/scintillationlysocecrystal>.
- [19] M. Martini, S. Paravisi, and C. Liguori, A new high sensitivity spectrometer for 3-D thermoluminescence analysis, *Radiation Protection Dosimetry* **66**, 447 (1996).
- [20] C. L. Melcher, J. S. Schweitzer, C. A. Peterson *et al.*, in *Proceedings of SCINT'95, Delft, Netherlands, 1995*, edited by P. Dorenbos and C. W. Van Eijk (Delft University Press, Delft, Netherlands, 1996), p. 309.
- [21] V. Bondar, L. Nagornaya, V. Martynov, I. Babychuk, N. Starzhinsky, K. Katrunov, B. Grunov, V. Baumer, G. Onishchenko, V. Krivoshein, and Yu. Malyukin, in *Proceedings of the SCINT'2005, International Conference on Inorganic Scintillators, and their Applications, Alushta, Ukraine, 2005*, edited by A. Gektin and B. Grinyov (Institute for Scintillation Materials, Alushta, Ukraine, 2005), p. 98.
- [22] S. W. S. McKeever, *Thermoluminescence of Solids, Cambridge Solid State Science Series* (Cambridge University Press, Cambridge, England, 1985).
- [23] D. Curie, *Luminescence in Crystals* (Wiley, New York 1960).
- [24] A. Gektin, A. Belsky, and A. Vasil'ev, Scintillation efficiency improvement by mixed crystal use, *IEEE Trans. Nucl. Sci.* **61**, 262 (2014).
- [25] M. Fasoli, A. Vedda, M. Nikl, C. Jiang, B. P. Uberuaga, D. A. Andersson, K. J. McClellan, and C. R. Stanek, Band-gap engineering for removing shallow traps in rare-earth $\text{Lu}_3\text{Al}_5\text{O}_{12}$ garnet scintillators using Ga^{3+} doping, *Phys. Rev. B* **84**, 081102(R) (2011).
- [26] K. Kamada, T. Endo, K. Tsutumi, T. Yanagida, Y. Fujimoto, A. Fukabori, A. Yoshikawa, J. Pejchal, and M. Nikl, Composition engineering in cerium-doped $(\text{Lu}, \text{Gd})_3(\text{Ga}, \text{Al})_5\text{O}_{12}$ single-crystal scintillators, *Cryst. Growth Des.* **11**, 4484 (2011).
- [27] M. Nikl, K. Kamada, V. Babin, J. Pejchal, K. Pilarova, E. Mihokova, A. Beitlerova, K. Bartosiewicz, S. Kurosawa, and A. Yoshikawa, Defect engineering in Ce-doped aluminum garnet single crystal scintillators, *Cryst. Growth Des.* **14**, 4827 (2014).
- [28] Y. Wu, F. Meng, Q. Li, M. Koschan, and C. L. Melcher, Role of Ce^{4+} in the Scintillation Mechanism of Codoped $\text{Gd}_3\text{Ga}_3\text{Al}_2\text{O}_{12}:\text{Ce}$, *Phys. Rev. Applied* **2**, 044009 (2014).
- [29] C. Greskovich and S. Duclos, Ceramic scintillators, *Annu. Rev. Mater. Sci.* **27**, 69 (1997).
- [30] Scintillation properties, <http://scintillator.lbl.gov/>.
- [31] E. D. Bourret-Courchesne, G. A. Bizarri, R. Borade, G. Gundiah, E. C. Samulon, Z. Yan, and S. E. Derenzo, Crystal growth and characterization of alkali-earth halide scintillators, *J. Cryst. Growth* **352**, 78 (2012).
- [32] M. Ishii, K. Harada, Y. Hirose, N. Senguttuvan, M. Kobayashi, I. Yamaga, H. Ueno, K. Miwa, F. Shiji, F. Yiting M. Nikl, and X. Q. Feng, Development of $\text{BSO}(\text{Bi}_4\text{Si}_3\text{O}_{12})$ crystal for radiation detector, *Opt. Mater.* **19**, 201 (2002).
- [33] E. Auffray, A. Borisevitch, A. Gektin, Ia. Gerasymov, M. Korjik, D. Kozlov, D. Kurtsev, V. Mechinsky, O. Sidletskiy, and R. Zoueyski, Radiation damage effects in $\text{Y}_2\text{SiO}_5:\text{Ce}$ scintillation crystals under γ -quanta and 24 GeV protons, *Nucl. Instrum. Methods Phys. Res., Sect. A* **783**, 117 (2015).
- [34] N. J. Cherepy, G. Hull, A. Droshoff, S. Payne, E. van Loef, C. Wilson, K. Shah, U. Roy, A. Burger, L. Boatner, W.-S. Choong, and W. Moses, Strontium and barium iodide high light yield scintillators, *Appl. Phys. Lett.* **92**, 083508 (2008).
- [35] D. J. Singh, Antisite defects and traps in perovskite YAlO_3 and LuAlO_3 : Density functional calculations, *Phys. Rev. B* **76**, 214115 (2007).
- [36] Yu. Zorenko, V. Gorbenko, I. Konstankevych, A. Voloshinovskii, G. Stryganyuk, V. Mikhailin, V. Kolobanov, and D. Spassky, Single-crystalline films of Ce-doped YAG, and LuAG phosphors: Advantages over bulk crystals analogues, *J. Lumin.* **114**, 85 (2005).
- [37] T. Q. Khan, P. Bodrogi, Q. T. Vinh, and H. Winkler, *LED Lighting: Technology and Perception* (John Wiley & Sons, New York, 2014).
- [38] Stanley R. Rotman, *Wide-Gap Luminescent Materials: Theory and Applications* (Springer Science & Business Media, New York, 1997).
- [39] J. Ruiz-Fuertes, S. Lopez-Moreno, J. Lopez-Solano, D. Errandonea, A. Segura, R. Lacombe-Perales, A. Munoz, S. Radescu, P. Rodriguez-Hernandez, M. Gospodinov, L. L. Nagornaya, and C. Y. Tu, Pressure effects on the electronic and optical properties of AWO_4 wolframites ($A = \text{Cd}, \text{Mg}, \text{Mn},$ and Zn): The distinctive behavior of multiferroic MnWO_4 , *Phys. Rev. B* **86**, 125202 (2012).
- [40] D. J. Singh, Structure and optical properties of high light output halide scintillators, *Phys. Rev. B* **82**, 155145 (2010).
- [41] A. Chaudhry, R. Boutchko, S. Chourou, G. Zhang, N. Grønbech-Jensen, and A. Canning, First-principles study of luminescence in Eu^{2+} -doped inorganic scintillators, *Phys. Rev. B* **89**, 155105 (2014).
- [42] A. F. Lima, S. O. Souza, and M. V. Lalic, Electronic structure and optical absorption of the $\text{Bi}_4\text{Ge}_3\text{O}_{12}$ and the $\text{Bi}_4\text{Si}_3\text{O}_{12}$ scintillators in ultraviolet region: An ab-initio study, *J. Appl. Phys.* **106**, 013715 (2009).
- [43] M. Nikl and A. Yoshikawa, Recent R&D trends in inorganic single-crystal scintillator materials for radiation detection, *Adv. Opt. Mater.* **3**, 463 (2015).
- [44] C. Dujardin, C. Pedrini, J. C. Gacon, A. G. Petrosyan, A. N. Belsky, and A. N. Vasil'ev, Luminescence properties and scintillation mechanisms of cerium- and praseodymium-doped lutetium orthoaluminate, *J. Phys. Condens. Matter* **9**, 5229 (1997).